Planetary and Space Science 229 (2023) 105660

Contents lists available at ScienceDirect

Planetary and Space Science

journal homepage: www.elsevier.com/locate/pss

On the origins of backscattered solar wind energetic neutral hydrogen from the Moon and Mercury

F. Leblanc [a,*], R. Deborde [a], D. Tramontina [b], E. Bringa [b], J.Y. Chaufray [c], S. Aizawa [d], R. Modolo [c], L. Morrissey [e], A. Woodson [f], S. Verkercke [a], C. Dukes [f]

[a] LATMOS/CNRS, Sorbonne Université, Paris, France
[b] CONICET, Facultad de Ingeniería, Universidad de Mendoza, Mendoza, 5500, Argentina
[c] LATMOS/CNRS, Université Versailles Saint Quentin, Guyancourt, France
[d] IRAP, Toulouse, France
[e] Memorial University, Canada
[f] University of Virginia, Charlottesville, USA

A B S T R A C T

The surfaces of planetary airless bodies are directly bombarded by solar particles. The most abundant of those particles are solar wind protons. In the case of the Moon, many in situ observations have shown that a significant portion of these incident solar-wind protons are backscattered as energetic neutral hydrogen atoms (ENA). Measurements of the energy flux distribution of these neutral particles provide a clue regarding the processes occurring in the surface regolith when impacting protons collide with the surface grains.

In this work, we developed a model to describe the fate of protons through a regolith model and compared our results with Chandrayaan-1 ENA measurements. We combined a Monte Carlo approach to reconstruct the motion of these particles into a layer of grains with molecular dynamics to parametrize the interaction of an incident proton with a grain. Using simultaneous measurements of the incident plasma by Chandrayaan-1 SWIM, this detailed modelling allowed us to analyse the measurements performed by the Chandrayaan-1 CENA instrument when the Moon is in the solar wind and in the Earth's magnetosheath, and to highlight what could control the flux and energy properties of these backscattered neutral hydrogen particles. Predictions of the intensity and shape of the backscattered neutral hydrogen distribution at Mercury are derived from this calculation.

1. Introduction

The surfaces of planetary airless bodies, such as the Moon, are directly bombarded by solar wind protons, giving rise to surface bound exospheres (Stern, 1999). IBEX-HI (McComas et al., 2009) observed that a significant portion of these incident protons (between 10 and 20%) are backscattered from the Moon as Energetic Neutral Atoms (ENA). The global value was later confirmed to be 9% using the IBEX-Lo (Rodríguez et al., 2012; Funsten et al., 2013; Allegrini et al., 2013) instrument on board the IBEX mission. Using the Chandrayaan-1 Energetic Neutral Atom Instrument (CENA) sensor of the Sub-keV Atom Reflecting Analyzer (SARA, Barabash et al., 2009) on board the Chandrayaan-1 Lunar orbiter (Goswami and Annadurai,2009), Wieser et al. (2009) estimated that up to 20% of the solar wind protons incident on the Lunar equator might be backscattered as ENAs, a value which was later confirmed as being equal to 19% by Futaana et al. (2012). Vorburger et al. (2014) also reported that backscattered He neutral atoms amount to only 0.14% of the total number of incident He^{++} solar wind ions. Based on IBEX measurements, Funsten et al. (2013) reported an ENA albedo varying from 20% for slow solar wind to 8% for fast solar wind, a value confirmed by Allegrini et al. (2013) who found a value of 10% on an average.

These backscattered ENAs essentially follow a Solar Zenith Angle (SZA) dependency (Wieser et al., 2009; Saul et al., 2013) directly proportional to the incident solar wind proton flux with the exception of the regions of local crustal magnetic fields. In these particular regions, Chandrayaan-1/CENA instruments observed a complex spatial structure of the reflected backscattered protons suggesting that the incident solar wind flow is deflected by the local magnetic field anomaly (Futaana et al., 2013). Backscattered ions were also observed by SELENE/MAP-PACE (Saito et al., 2008) corresponding to a percentage of the incident solar wind protons between 0.1 and 1%, a value later confirmed by ARTEMIS (Lue et al., 2018) which reported the percentage of backscattered protons between 0.5% for a solar wind speed of 300 km/s and 0.3% for a solar wind speed of 500 km/s.

In Futaana et al. (2012) and Wieser et al. (2009), a measurement of

* Corresponding author.
E-mail address: francois.leblanc@latmos.ipsl.fr (F. Leblanc).

https://doi.org/10.1016/j.pss.2023.105660
Received 16 November 2022; Received in revised form 3 February 2023; Accepted 2 March 2023
Available online xxxx
0032-0633/

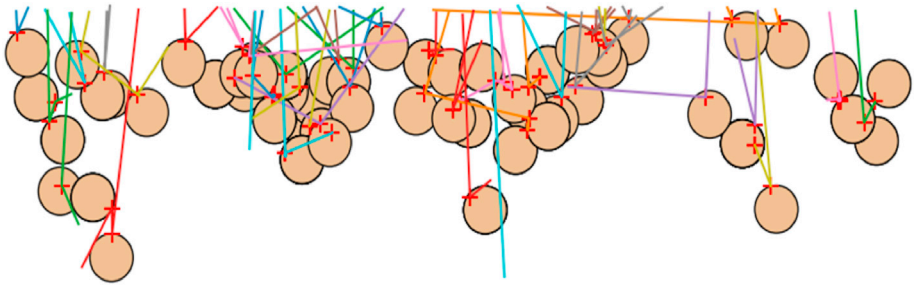

Fig. 1. Cut along a vertical slice of the modeled regolith displaying the trajectories of several test-particles through a regolith composed of grains of 1.52 μm diameter (brown circles) with a density of 35%. The red crosses represent the position of the impact of each test-particle on a grain surface.

the differential energy flux of the backscattered hydrogen ENAs was provided by Chandrayaan-1/CENA covering an energy range from 25 eV up to 10 keV on three consecutive orbits in July 2009 and February 2009. Futaana et al. (2012) used observations performed when the Moon was in the solar wind whereas Wieser et al. (2009) used data observed in the magnetosheath of the Earth. Despite a difference in flux of one order of magnitude, both distributions peak around 200 eV, an energy much larger than for hydrogen atoms that would be sputtered from the surface (Behrisch and Eckstein, 2007), with an extended plateau from 200 eV to the lowest energy covered by CENA and a quick decrease of the flux from 200 eV up to a few keV (to be compared to the typical 1 keV energy of the incident solar wind protons). Such distribution was interpreted by Futaana et al. (2012) as the evidence of "*multiple collisions off surfaces of regolith grains*". Wieser et al. (2009) measured an ENA backscattered flux larger than Futaana et al. (2012) in agreement with the conclusions by Allegrini et al. (2013) showing that ENA backscattered fluxes measured in the magnetosheath are larger on average than the same flux measured when the Moon is in the Solar wind. Allegrini et al. showed that back scattering hydrogen fluxes were more intense in the magnetosheath for energies below ~0.6 times the Solar Wind energy by analyzing many spectra of the IBEX sensors normalized by the average conditions. These authors concluded that higher low-energy release occurs when the plasma Mach number is lower. Rodríguez et al. (2012), using IBEX/IBEX-Lo, reported a similar energy distribution of the hydrogen ENAs with an extended plateau down to the limit of detection of IBEX-Lo at 14 eV when the Moon was in the Solar Wind or in the magnetosheath. We are not aware of any measurement by IBEX or Chandrayan-1 of ENA when the Moon is inside the Earth magnetosphere. More recently, Zhang et al. (2020) using the Advanced Small Analyzer for Neutrals on board the Chinese CHang'E−4 rover reported a hydrogen ENA albedo of 32% above 30 eV.

Hodges (2011) published the first complete modelling of the interaction of solar wind protons with a regolith using a Monte Carlo approach that followed atoms in the Lunar surface, including representative solar wind fluxes. That study stated a neutralization probability of the impacting protons equal to 91% to fit with the observed 1% of particles reflected as ions (Saito et al., 2008) and a 45% average energy loss during each collision between an incident atom and a grain. Hodges (2011) completed a detailed analysis of the measurements reported by Wieser et al. (2009) and found an excellent agreement between simulation and observations taking into account some corrections (Wieser et al., 2011) to the originally published (Wieser et al., 2009) differential energy flux and Chandrayaan-1/CENA instrumental energy response.

In this paper, we employ a similar approach as Hodges (2011) by modelling incident solar wind particles penetrating a regolith model to reproduce Chandrayaan-1/CENA measurements. However, in this study we use a combined Monte Carlo/Molecular Dynamics approach. First, Monte Carlo modelling is used to reconstruct the motion of these particles into a layer of grains representative of the lunar surface regolith. Next, we then use molecular dynamics (MD) to properly describe the interaction of an incident proton with a grain—in particular the energy loss and angular redistribution during particle-grain collisions. This detailed modelling approach allows us to accurately analyse the measurements performed by the Chandrayaan-1 CENA instrument and to highlight what could control the flux and the energy of these backscattered hydrogen atoms. We also extrapolate the results of this modelling in order to predict what should be the observed flux of hydrogen ENA at Mercury (Lue et al., 2017; Orsini et al. 2021). Section II describes the two models used to perform our modelling whereas section III presents the results of this modelling and section IV concludes this paper.

2. Model

The model developed to describe the fate of the solar wind protons in the upper layer of the Lunar surface can be decomposed into two parts:

- a calculation of the trajectory of an individual particle in a layer composed of grains (defined as single-crystal unit within a poly-crystalline material, section II.1),
- a calculation of the interaction of a particle with a grain (section II.2)

2.1. The fate of protons through a regolith

The regolith is described by an ensemble of 70000 spherical grains with a diameter of 1.52 μm in 70 μm^3, yielding a density of ~35%, which is close to the expected grain density at the Moon's surface (Sarantos and Tsavachidis, 2021). Typical distance between grains is of the order of 3 μm. This size of grain is small with respect to the typical size of grain at the Moon surface (Sarantos and Tsavachidis, 2021), but might be representative of the top layer of the surface. Such an effect will be addressed in a forthcoming paper.

To be able to compare directly our results to data deduced from Chandrayaan-1/CENA measurements, we used Chandrayaan-1/SWIM energy distribution of the incident solar wind protons measured simultaneously for three orbits on the February 6, 2009 (Wieser et al., 2011) but corrected by a factor 0.55 as suggested by Hodges (2011) based on a comparison between SWIM and ACE measurements. For Futaana et al. (2012), typical solar wind conditions during the 17 and July 18, 2009 corresponded to a mean solar wind speed of 290–320 km/s and a solar wind density of 4.8–6.0 cm^{-3}. The solar wind conditions are used to generate individual proton test-particles, each of them representative of a large number of real particles as defined by a weight. The initial velocity of these test particles is determined from a mean solar wind bulk velocity component pointing towards the surface (radial direction) to which an isotropic thermal velocity component is added. The trajectory of the particle is calculated below the surface up to the moment the particle either reemerges from the surface—in which case we registered its velocity, weight and charge—or reaches an energy smaller than 10 eV. At each time step we determine if the particle encounters a grain (see Fig. 1), in which case a parameterization based on the molecular dynamics

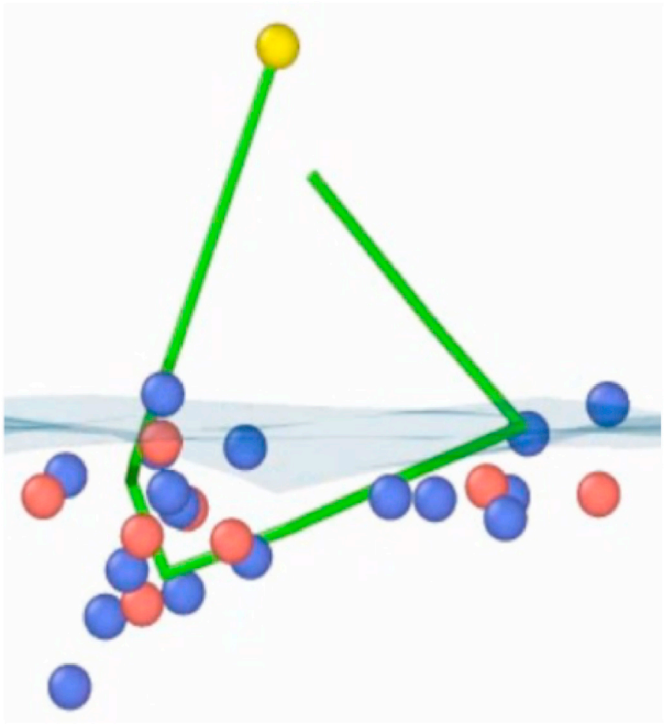

Fig. 2. Trajectory (green lines) of a proton (yellow atom) interacting with a SiO_2 regolith grain. The blue circles represent O atoms whereas the red circles represent Si atoms. The typical spatial scale of this trajectory is few nm. This trajectory is significantly different from the often assumed single specular collision. Only atoms acquiring an energy larger than 0.2 eV are shown.

modelling described in section II.2 is used to determine the energy and velocity direction of the reemitted particle. We neglect the effects of the gravity fields of the Moon and the Earth as well as any electro-magnetic forces that could act on the trajectory of the particle. Indeed, since the typical distance between two collisions is of only few μms (equivalent to the inter-granular distance), the true trajectory between two collisions would closely approximate a straight line. Moreover, for the energy range considered in this work (between 10 eV and few keV), the change in energy is largely dominated by particle-grain collisions, while that due to gravity and electro-magnetic fields is negligible. The time step was optimized to reduce the calculation duration but was also kept small enough to properly describe all collisions between particle and grain (typically of the order of 0.3 ps). The timestep was also adjusted to determine accurately the position of each grain-particle collision at the surface of the grains.

To describe the trajectory of a test particle just after its collision with a grain, we need to define several parameters:

- the position of the impact at the surface of the grain and the velocity of the test particle in the frame of the grain;
- the charge state of the particle, for which we used Hodges (2011) assumption that neutralization is very efficient and corresponds to a probability of 91% that an incident ion will be neutralized after encountering the regolith;
- the probability that a particle is implanted or absorbed into the grains (section II.2), which is taken into account by reducing the weight of the test-particle by the percentage absorbed in the grain;
- the energy of the particle after collision, determined using a Molecular Dynamics model (see section II.2),
- the direction of the velocity vector after collision, which is determined by the Molecular Dynamics model as described in section II.2.

Thus, when a particle collides with a grain, the new velocity vector of the particle is calculated at the position of the impact of the particle with the grain, neglecting the nanometer distance travelled by the particle into the grain.

2.2. Grain – proton interactions

To account for proton-grain interaction, we used an atomistic Molecular Dynamics model that describes the proton interaction with a grain composed of a set of atoms as illustrated in Fig. 2.

Classical molecular dynamics simulations solve Newton's equations for a set of interacting particles. We use the open-sourced software LAMMPS (Thompson and M Aktulga, 2022) to model the impact of protons on a silica surface. Interactions between atoms are described by Reactive Force Field (ReaxFF; Smith et al. 2017), which includes several different contributions like screened Coulomb interactions, and allows for charge exchange and various bonding environments. ReaxFF has been extensively used for silica simulations (Fogarty and Aktulga, 2010, Yu and Wang, 2016; Joseph and Swaminathan, 2021). We use a standard procedure to build a silica sample, starting from a quartz crystal, molten, then cooled, and finally relaxed to obtain a glassy sample. Details of this procedure are given in the Supplementary Material (SM). The final density of this amorphous sample is 2.21 g/cm^3, in agreement with experiments (Quenneville et al., 2010) and simulation results (Fogarty and Aktulga, 2010). The partial correlation functions $g_{ij}(r)$ shown in SM Fig. S1, compare extremely well with the ones obtained previously by similar simulations (Nayir et al., 2019; Onodera, 2020). In order to simulate bombardment, a free surface is created by generating a vacuum region above the sample, and then relaxing that new structure. This leads to some reconstruction at the surface, as expected. The final sample is approximately a cube, 7 nm side, and has 24000 atoms (8000 Si, 16000 O). Lateral periodic boundary conditions were used. Atoms in the bottom 0.2 nm were fixed, and the velocity of protons reaching this layer was set to zero, in order to mimic a much deeper regolith sample. There is approximately 1.5 nm of vacuum above and below the sample, to model bombardment.

Incident protons are approximated as neutral hydrogen atoms. We found that reflection typically involves many collisions in the upper few nm of the silica sample, and fast neutralization is expected, as discussed above, at this low impact energy. Due to the high computational cost of charge exchange, it was included in the sample preparation, but we turned this off during the thousands of impact simulations carried out. This set-up neglects backscattering of H^+, which is expected to be more than one order of magnitude lower than H backscattering. Random impact points are selected for each bombardment, leading to different local environments around the impact and various outcomes, including the possibility of reflection and sputtering of target atoms. MD simulations were carried out adding a close range Ziegler, Biersack and Liitmark potential (ZBL; Ziegler, 2004) to ReaxFF, for atoms closer than 0.1 nm. Details about the implementation of ZBL appear in Appendix 1. Simulations used an adaptive time step, and finished after about 2 ps, when the proton reached the bottom of the sample and was considered absorbed, or when it was reflected and reached the top of the simulation box. 500 events were simulated for each (energy, angle) combination. This was enough to ensure reflection coefficients with an error of less than 10%. We simulated independent impacts, always with the same pristine sample, but changing the impact site for a given impact energy and angle. Future studies might include cumulative impacts where incident ions change the nature of the target. Fig. 2 shows the outcome of a typical single simulation.

In order to fully characterize the proton-grain collisions, we need to specify three parameters, as follows:

- For each of the simulated energies/angles, we computed the number of protons reflected from the grain (see as an example Fig. 2). Five sets of simulations were performed at 25 eV, 50 eV, 200 eV, 500 eV, 800 eV and 1200 eV, for an incident angle of 45° (Fig. 3a). The

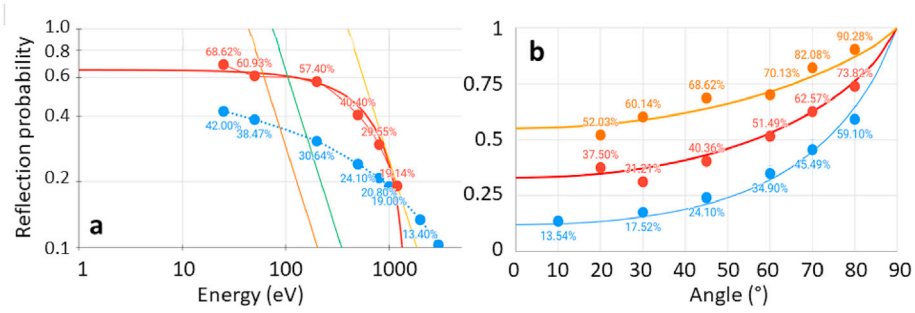

Fig. 3. Panel a: Reflection probability of a proton colliding with a grain as a function of its incident energy at an angle of 45° with respect to the surface normal. MD simulations (red circles), SRIM (blue circles, joined by a dotted line), and proposed fit using Eq. (1) (thick solid red line). WS model fits, assuming different targets (thin solid lines): SiO_2 (orange), Si (green), O (yellow). Panel b: Reflection probability as a function of the incident angle using SRIM (500 eV protons, blue) and MD simulations (500 eV, red circles, and 25 eV, orange circles). Lines correspond to fits with a BW model (Bøttiger et al., 1973). $R_0 = 0.12$, $b = 0.9$ (blue line). $R_0 = 0.33$, $b = 0.8$ (red line), and $R_0 = 0.25$, $b = 0.83$ (orange line).

dependency of this reflection with respect to the energy was then deduced and fitted with a function described below. Simulations for several angles in the range 20–80° were performed at 25 eV and 500 eV, in order to derive angular dependency, see Fig. 3b. Combining the two dependencies, we found a best fit of the reflection probability with respect to both incident angle θ and energy E following:

$$P_{reflection}(\theta, E) = \left(0.603 \times e^{-1.372\times10^{-3}\times E}\right)^{(cos\theta)^{0.8}} \quad (1)$$

Fig. 3 includes simulations using SRIM2013. We obtained results using 10^5 protons, impacting a regolith of density of 2.21 g/cm^3 with a lattice binding energy of 1 eV for Si and 8 eV for O, and a surface binding energy for Si and O atoms of 0.5 eV. These binding energies were chosen to reproduce mean values in the MD simulations, where there is a wide distribution of lattice and surface binding energies, as recently discussed for Na in a silicate (Killen et al., 2022). SRIM2013 results are 30%–50% lower than MD results at low energy, but there is a cross-over near 1.2 keV. SRIM cross-sections were derived from experimental results starting at a few keV, and are not expected to be reliable below a few keV [Posselt and Heinig 1995]. Binary Collision Approximation (BCA) codes like SRIM suffer from difficulties describing surface structure and binding, although there are improvements with respect to SRIM2013 (Szabo et al., 2022).

Fig. 3a also includes the WS model (Weissmann and Sigmund, 1973) for which the reflection probability R follows $R = 1.05 \times \varepsilon^{-3/2}$ *with* $\varepsilon = \left(\frac{M_2 E}{M_1+M_2}\right) \Big/ \left(\frac{Z_1 Z_2 e^2}{a}\right)$ *with* M_1, M_2, Z_1, Z_2, a, *and* e being the mass of the proton, the mass of the molecules in the regolith, the atomic number of the proton, the atomic number of the molecules in the regolith, the Bohr radius and the elementary charge respectively. The WS model assumes a single bouncing collision for reflection and is intended as a rough guide only. Reflection probability goes to 1 as energy goes down, and this requires the inclusion of multiple collisions. Thomas et al. (1992) proposed an alternative equation for R in terms of scaled energy, but it requires six different fit parameters. Fig. 3b also includes SRIM results for 500 eV. For 25 eV incident energy SRIM would be unreliable at energies so close to the binding energy, where many-body, not binary, collisions would be crucial, and no results are included. Note that the decrease of reflection as angle decreases is stronger for BCA than for MD simulations. We also show lines corresponding to a Bøttiger-Winterbon (BW) model of the form $R = R(\theta{=}0)^{\cos(\theta)^{*}b}$, with $b = 0.8$ for MD simulations and $b = 0.9$ for SRIM. Discrepancies between BCA codes and experimental sputtering yields for H against SiO_2 were noted in a recent study (Schaible et al., 2017).

- If the particle is re-ejected from the grain, we estimated its energy after collision using the simulated energy distribution of the backscattered protons derived from four simulations performed at an angle of 45° for 25 eV, 200 eV, 500 eV and 800 eV (Fig. 4). We linearly interpolated between these four profiles to derive the energy of the re-ejected particles for any incident energy.

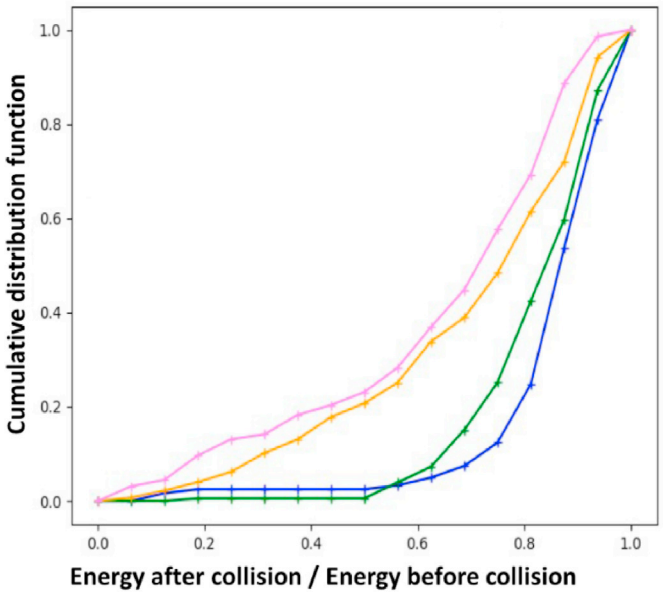

Fig. 4. Cumulative energy distribution of a hydrogen atom reflected from a single regolith grain. Blue, green, orange and pink lines are for 800 eV, 500 eV, 200 eV and 25 eV incident proton energy at 45°.

- The last parameter needed to fully describe the velocity vector of the backscattered particle is its angle with respect to the normal to the surface. Here again, according to the results obtained with the Molecular Dynamics simulations, below 60° incident angle of the incident primary or secondary particles with respect to the normal to the surface, we used a Gaussian function centered around the incident angle and with a Full Width Half Maximum (FWHM) of 18° whereas above 60° a Rayleigh distribution centered on the incident angle and with a FWHM following a relation like $\sigma(\theta) = -0.0163\theta + 1.48$ is used.

3. Results

3.1. Hydrogen Energetic Neutral Atoms backscattered from the Moon surface

Approximately 700000 test particles were tracked for each simulation, incorporating Futaana et al. solar wind conditions and Wieser et al. Magnetosheath conditions for which 20.4% and 18.9% of the test particles were reflected while 79.6% and 80.8% were absorbed respectively. In both cases, less than 1% of protons reached energies lower than 10 eV before being absorbed. Each test particle underwent 4 collisions with the grain, on average, before exiting the simulation and the maximum penetration depth was of only 20 μm with more than 95% of the incident protons being deposited at a regolith depth less than 6 μm.

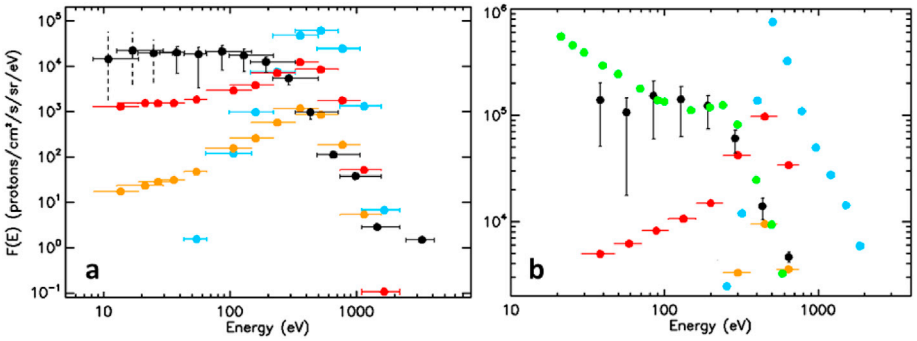

Fig. 5. Panel a: black points: measured differential energy flux of ENA by Chandrayaan-1/CENA (Futaana et al., 2012). Red points: simulated differential energy flux of backscattered H from the Moon surface. Blue points: measured solar wind incident proton differential energy flux (Chandrayaan-1/SWIM, Futaana et al., 2012). Orange points: simulated differential energy flux of backscattered protons. Panel b: black points: measured differential flux of ENA by Chandrayaan-1/CENA (Wieser et al., 2011). Red point: simulated differential energy flux of backscattered H from the Moon surface. Blue point: measured solar wind incident proton differential energy flux (Chandrayaan-1/SWIM, Wieser et al., 2011). Orange point: simulated differential energy flux of backscattered protons. Green points: simulated differential energy flux by Hodges (2011).

In Fig. 5 we show the differential energy flux of hydrogen ENA as measured by the Chandrayaan-1/CENA instrument and reported by Futaana et al. (2012) (black points in panel a) and Wieser et al. (2011) (black points in panel b). CENA measurements below 30 eV are shown even if reported by Futaana et al. (2012) as highly uncertain. Our simulated fluxes of hydrogen ENA are shown in red and our simulated proton backscattered fluxes in orange. We simply summed in each energy band of CENA the weight of the particle divided by the energy width and by 2π steradian (assuming an isotropic ejection). We also reproduced the solar wind proton flux used for both simulations in blue. The simulated proton backscattered fluxes might be influenced by the charge state of the surface (Halekas et al., 2010), in particular at low energy, the dayside surface potential being able to reach few tens of V.

As shown in Fig. 5, we found a better agreement between simulation (red symbols) and observation (black symbols) in the case of the observation performed when the Moon was in the Solar Wind (panel a) than when the Moon was in the magnetosheath (panel b). As a matter of fact, both measured fluxes are surprisingly similar in shape despite different incident protons fluxes. Hodges (2011) modeled the panel b case using a corrected Solar Wind flux, decreased by a factor 0.55 over that of Wieser et al. (2011)—a correction we also adopted for the panel b simulation. The flux measured by SWIN on board Chandrayaan-1 and displayed in blue points on Fig. 5b and used to simulate the backscattered flux is therefore probably not accurate enough and might explain part of the discrepancy between observation and simulation. In Fig. 5 panel b, we also plot the simulated differential energy flux of the backscattered hydrogen atoms as modeled by Hodges (2011). The very good agreement between the observation and Hodges model was obtained by adopting a mean energy loss of 45% at each collision, an energy loss not predicted by our Molecular Dynamics simulation as displayed in Fig. 4. The backscattered flux simulated by our model (red points) peaks at the right order of magnitude around 200 eV and decreases at a rate close to that observed for energies $>$ 200 eV. However, our simulation displays a decrease of the backscattered population at lower energies that is not seen in the observation nor in Hodges (2011) simulation. As a matter of fact, Futaana et al. (2012) pointed out that the 60% rate for backscattered hydrogen ENA above 25 eV suggested by Hodges (2011) was not consistent with their estimated range of 9–24%, which is in good agreement with our present estimate. This suggests that a scenario with an increased intensity of the differential flux below 100 eV is less likely. Moreover, IBEX reported several observations with better sensitivity at low energy than CENA suggesting the existence of such a plateau in the Solar Wind (Allegrini et al., 2013), a suggestion reinforced by the most recent measurements by ASAN/Chang'E 4 (Zhang et al., 2020). The origin of this plateau in flux below 200 eV appears to be partly associated with the Solar Wind flux distribution. Comparing the simulated back-scattered hydrogen energy distribution displayed in Fig. 5a to the simulated one in Fig. 5b, there is a clear difference in the shape of the backscattered distribution at low energy. The main difference between these two simulations being the input Solar Wind distribution, it is clearly one of the parameters controlling the shape of the backscattered distribution at low energy. This plateau should also be populated by back-scattered hydrogen atoms coming from incident Solar Wind protons that lost a significant part of their energy through the regolith. Since our simulation clearly underestimates this plateau, it implies that we do not succeed in properly describing this population of particles losing more than 80% of their initial energy before being reemitted. One possible explanation is our choice to describe the surface upper layer with smaller grains than are actually present on the Moon's surface. Both grain size and aggregation porosity will affect backscattering (Szabo et al., 2022). This concern will be explored further in a forthcoming paper.

Allegrini et al. (2013) also highlighted that the energy peak of the backscattered neutral hydrogen flux usually occurred at an energy equal to 60% of the Solar Wind incident energy. In the case of the measurements done when the Moon was in the Solar wind (Fig. 5a), the Solar Wind flux peaked at an energy around 500 eV and our simulated backscattered flux peaked at an energy of 320 eV, in good agreement with the conclusion of Allegrini et al. (2013). In the case of the magnetosheath measurements (Fig. 5b), our simulation suggested a peak in energy of the backscattered hydrogen atoms slightly smaller than the incident energy (at 450 eV for an incident flux peaking at 500 eV). This suggests that, in our simulation, the energy at which the backscattered neutral flux peaks is not only related to the incident Solar wind energy but also to its temperature. The measured, backscattered-proton flux and the backscattered-proton flux modeled by Hodges (2011) both peaked at an energy equal to ~220 eV, significantly smaller than what we should have expected given the conclusion of Allegrini et al. (2013). This difference again suggests that the input used for our simulation displayed in Fig. 5b is probably not accurate enough.

Since energetic hydrogen atoms can also be produced through sputtering of the regolith by incident protons, we considered the possibility of a sputtered contribution to the observed CENA differential flux. Based on the study of Eckstein et al. (2007), we estimated the efficiency of hydrogen sputtering from the grains by incident protons to be the same as that for incident Li atoms. The angular distribution of the ejecta was chosen to follow a $\cos(\theta)$ relation while the energy distribution falls off as E^{-2} above 10 eV, which is the range of energy considered here. According to Eckstein et al. (2007), the yield varies from 0.2 at a normal incidence to a maximum of 2 around 75° incidence angle and is only marginally dependent on the incidence energy within the typical solar wind energy range. These values are rather large since classical values for the yield of protons impacting a regolith are closer to 0.1 (see as an example Schaible et al., 2017). Even for the very unrealistic case in which the hydrogen abundance in the grain is one, the sputtered population would not exceed 10^3 hydrogen atoms/(cm^2 s sr eV) at 10 eV and would quickly decrease for larger energy. Therefore, it is very unlikely that the observed flux has a significant contribution from sputtering as concluded also by Futaana et al. (2012).

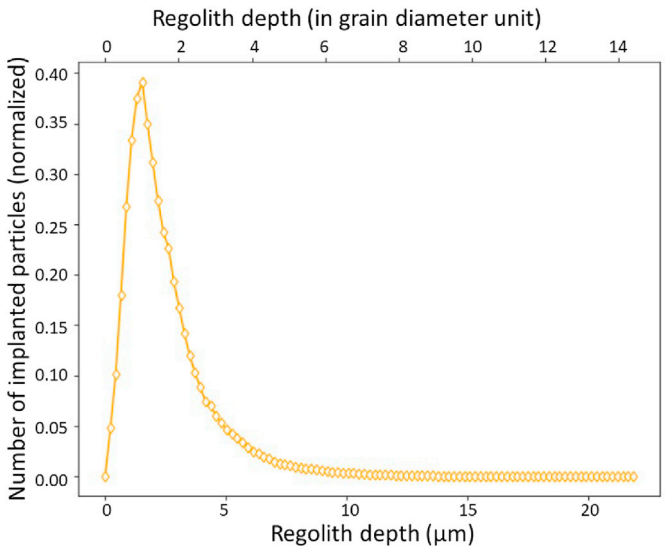

Fig. 6. Depth implantation of the incoming solar wind proton in the regolith. Horizontal lower scale in μm, horizontal top scale in grain diameter unit.

As stated above 83.5% of the incident protons are absorbed in the grain. Our model can provide a first estimate of the depth at which these incident protons will get implanted. According to Fig. 6, most of the protons are implanted in the first layer of grains between 0 and 5 μm below the surface. This result is consistent with the relatively limited number of collisions, on average, of the incident protons in the regolith.

3.2. *Hydrogen Energetic Neutral Atoms backscattered from Mercury surface*

Following the results of our modelling of the backscattered hydrogen ENA from the Moon surface, we simulated what could be the flux of backscattered hydrogen ENA from Mercury's surface. Aizawa et al. (2022) simulated the solar wind proton flux penetrating the magnetosphere of Mercury and impacting the planetary surface for various solar wind conditions. In Fig. 7, panel a, we displayed the flux of protons impacting the surface in the case of nominal solar conditions as simulated by Aizawa et al. (2022). From this flux and the energy and angular distributions of the reflected ENAs simulated on the Moon, we reconstructed the ejection rate and the energy and angular distributions of hydrogen ENA from the surface of Mercury. We used the same approach described in sections II.1 and II.2 with the assumption that both regoliths have similar albedo. In panel b of Fig. 7, the ratio of ejected hydrogen ENA to incident protons is displayed with values between 5% and 25%. When comparing panels a and b, we don't find a direct relation between impacting and backscattered flux because, as shown in Fig. 3, the rate of backscattered particles depends on the energy and angle of the incident particles.

In Fig. 7c, we reconstructed the potential rate of backscattered hydrogen ENA that could be measured at 400 km in altitude above Mercury's surface, the typical periapsis altitude of MPO/BepiColombo (see appendix 2 regarding the mathematical approach used for this calculation). As shown on this panel, the shape of the simulated hydrogen ENA does not accurately reflect panels a and b. It is a spatially blurred image of the precipitation flux at the surface of Mercury (panel d), essentially because the ENAs flux comes from a large portion of the surface, but probably less blurred than an image of the precipitation that could be reconstructed from magnetic field measurements at 400 km above the surface, highlighting the interest of ELENA/SERENA on board BepiColombo (Orsini et al. 2021).

4. Conclusion

Solar wind protons have been observed to be back-scattered from the Moon's surface by the Chandrayaan-1 ENA instrument (Wieser et al., 2009; Futaana et al., 2012) as well as by the IBEX Lo instrument (McComas et al., 2009), showing an unexpected high rate of protons backscattered as neutral hydrogen atoms. The Chandrayaan-1 ENA instrument was also able to measure the energy distribution of these particles simultaneously with measurements of the solar wind characteristics.

Using this information, we developed a model describing the fate of protons moving through a Lunar regolith approximated as individual spherical grains. Our model combined a Monte Carlo approach that tracks the motion of atoms in the upper 10–20 μm of the regolith with a

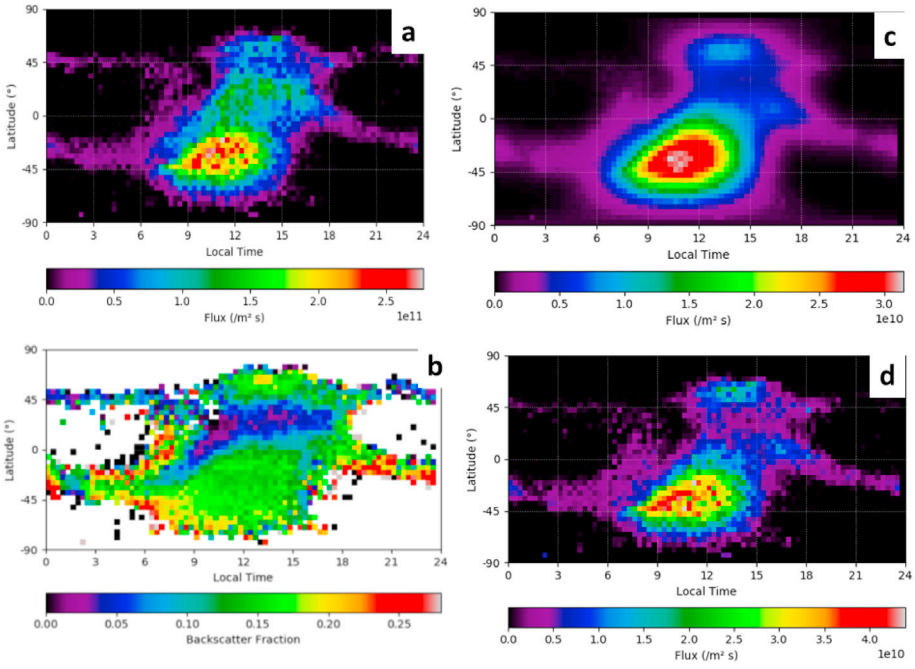

Fig. 7. Panel a: Precipitating flux of H^+ Solar Wind particles impacting the surface for nominal solar wind conditions, a Solar Wind speed of 450 km/s, a Solar Wind density of 50 cm^{-3} and an Interplanetary Magnetic Field of 17 nT with nominal Parker Spiral orientation at Mercury (Aizawa et al., 2022). Panel b: Backscattered fraction of the incident protons as hydrogen ENA (taking into account incident energy and angle of the incident protons). Panel c: reconstructed hydrogen ENA flux at 400 km in altitude. Panel d: backscattered flux of proton at the surface.

Molecular Dynamics approach describing the interaction between individual atoms and grains. Our model reproduced Chandrayaan-1/ENA observations with good agreement in the case of those measurements obtained in the Solar Wind (Futaana et al., 2012), while agreement was less pronounced and in a lesser way in the case of those measurements obtained in the magnetosheath (Wieser et al., 2009).

Lastly, by applying our model to a map of Solar Wind proton precipitation at Mercury we have provided an estimate of backscattered atomic hydrogen flux at the planet's surface and at 400 km altitude, which will coincide with the BepiColombo/Mercury Planetary Orbiter nominal periapsis altitude, thus allowing direct comparison between our estimates and in orbits measurements once the spacecraft arrive at Mercury in 2025 (Saito et al., 2021).

Author statement

Leblanc F. and CHaufray J.Y.: Conceptualization, methodology and software. R. Deborde: Conceptualization, methodology and software of the MC part. Tramontina D. and Bringa E.: Conceptualization and software of the MD part. Aizawa S., Modolo R., Morrissey L., Woodson A., Verkercke S. and Dukes C.: supervision and validation.

Declaration of competing interest

The authors declare that they have no known competing financial interests or personal relationships that could have appeared to influence the work reported in this paper.

Data availability

Data will be made available on request.

Acknowledgments

F.L. and J.-Y.C. acknowledge the support by ANR, France of the TEMPETE project (grant ANR-17-CE31-0016) and the support of CNES, France for the BepiColombo mission. This research was supported by the International Space Science Institute (ISSI) in Bern, through ISSI International Team project # 559 “Improving the Description of Exosphere Surface Interface”. Authors also acknowledge the support of the IPSL data center CICLAD for providing us access to their computing resources and data. Data may be obtained upon request from F. Leblanc (email:francois.leblanc@latmos.ipsl.fr). EMB and DT thank support from PICTO-UUMM-2019-00048 and SIIP-UNCUYO 06/M008-T1.

Appendix A. Supplementary data

Supplementary data to this article can be found online at https://doi.org/10.1016/j.pss.2023.105660.

References

Aizawa, S., André, N., Persson, M., Modolo, R., Raines, J., Leblanc, F., Chaufray, J.-Y., Nenon, Q., 2022. Escape and precipitation of planetary ions at Mercury under different solar wind conditions. Planet. Space Sci. submitted for publication.

Allegrini, F., Dayeh, M.A., Desai, M.I., Funsten, H.O., Fuselier, S.A., Janzen, P.H., McComas, D.J., Möbius, E., Reisenfeld, D.B., Rodríguez, D.F.M., Schwadron, N., Wurz, P., 2013. Lunar energetic neutral atom (ENA) spectra measured by the interstellar boundary explorer (IBEX). Planet. Space Sci. 85, 232–242.

Barabash, S., Bhardwaj, A., Wieser, M., Sridharan, R., Kurian, T., Varier, S., Vijaykumar, E., Abhirami, V., Raghavendra, K.V., Mohankumar, S.V., Dhanya, D.B., Thampi, S., Asamura, K., Andersson, H., Futaana, Y., Holmstr€om, M., Lundin, R., Svensson, J., Karlsson, S., Piazza, R.D., Wurz, P., 2009. Investigation of the solar wind-Moon interaction on board Chandrayaan-1 mission with the SARA experiment. Curr. Sci. 96 (4), 526–532.

Behrisch, R., Eckstein, W., 2007. Sputtering by Particle Bombardment. Springer Berlin Heidelberg. https://doi.org/10.1007/978-3-540-44502-9.

Bøttiger, J., Winterbon, K.B., 1973. Reflection of light ions from solid surfaces. Radiat. Eff. 20, 65. https://doi.org/10.1080/00337577308232267.

Fogarty, J.C., Aktulga, H.C., et al., 2010. A reactive molecular dynamics simulation of the silica-water interface. J. Chem. Phys. 132, 174704. https://doi/oeg/0.1063/1.3407433.

Funsten, H.O., Allegrini, F., Bochsler, P.A., Fuselier, S.A., Gruntman, M., Henderson, K., Janzen, P.H., Johnson, R.E., Larsen, B.A., Lawrence, D.J., McComas, D.J., Möbius, E., Reisenfeld, D.B., Rodriguez, D., Schwadron, N.A., Wurz, P., 2013. Reflection of solar wind hydrogen from the lunar surface. Journal of Geophysical Research:Planets 118, 292. https://doi.org/10.1002/jgre.20055.

Futaana, Y., Barabash, S., Wieser, M., Holmström, M., Lue, C., Wurz, P., Schaufelberger, A., Bhardwaj, A., Dhanya, M.B., Asamura, K., 2012. Empirical energy spectra of neutralized solar wind protons from the lunar regolith. J. Geophys. Res.: Planets 117 (E5). https://doi.org/10.1029/2011je004019 n/a.

Futaana, Y., Barabash, S., Wieser, M., Lue, C., Wurz, P., Vorburger, A., Bhardwaj, A., Asamura, K., 2013. Remote energetic neutral atom imaging of electric potential over a lunar magnetic anomaly. Geophys. Res. Lett. 40, 262–266. https://doi.org/10.1002/grl.50135.

Goswami, J.N., Annadurai, M., 2009. Chandrayaan-1: India's first planetary science mission to the moon. Curr. Sci. 96, 4 25 February.

Halekas, J.S., Saito, Y., Delory, G.T., Farrell, W.M., 2010. New views of the lunar plasma environment. Planet. Space Sci. https://doi.org/10.1016/j.pss.2010.08.011.

Hodges, R.R., 2011. Resolution of the lunar hydrogen enigma. Geophys. Res. Lett. 38 (6). https://doi.org/10.1029/2011gl046688 n/a.

Joseph, E., Swaminathan, N., 2021. Investigation of mechanical properties and dispersion in silica/Styrene Butadiene Rubber (SBR) nanocomposites: a ReaxFF molecular dynamics study. Comput. Mater. Sci. 200, 110751. https://doi.org/10.1016/j.commatsci.2021.110751.

Killen, R.M., Morrissey, L.S., Burger, M.H., Vervack, R.J., Tucker, O.J., Savin, D.W., 2022. The influence of surface binding energy on sputtering in models of the sodium exosphere of Mercury. Planet. Sci. J. 3, 139. https://iopscience.iop.org/article/10.3847/PSJ/ac67de/pdf.

Lue, C., Futaana, Y., Barabash, S., Wieser, M., Bhardwaj, A., Wurz, P., Asamura, K., 2017. Solar wind scattering from the surface of Mercury: lessons from the moon. Icarus 296, 39–48. https://doi.org/10.1016/j.icarus.2017.05.019.

Lue, C., Halekas, J.S., Poppe, A.R., McFadden, J.P., 2018. ARTEMIS observations of solar wind proton scattering off the lunar surface. J. Geophys. Res.: Space Phys. 123, 5289–5299. https://doi.org/10.1029/2018JA025486.

McComas, D.J., et al., 2009. Lunar backscatter and neutralization of the solar wind: first observations of neutral atoms from the Moon. Geophys. Res. Lett. 36, L12104. https://doi.org/10.1029/2009GL038794.

Nayir, N., van Duin, A.C.T., Erkoc, S., 2019. Development of a ReaxFF reactive force field for interstitial oxygen in germanium and its application to GeO2/Ge interfaces. J. Phys. Chem. A 123, 43031. https://doi.org/10.1021/acs.jpcc.8b08862.

Onodera, et al., 2020. Structure and properties of densified silica glass: characterizing the order within disorder. NPG Asia Mater. 12, 85. https://doi.org/10.1038/s41427-020-00262-z.

Orsini, S., 120 colleagues, 2021. SERENA: particle instrument suite for determining the sun-mercury interaction from BepiColombo. Space Sci. Rev. 217. https://doi.org/10.1007/s11214-020-00787-3 insu-03108958.

Posselt, M., Heinig, K.-H., 1995. Comparison of BC and MD simulations of low-energy ion implantation. Nucl. Instrum. Methods Phys. Res. Sect. B Beam Interact. Mater. Atoms 102, 1. https://doi.org/10.1016/0168-583X(95)80148-F.

Quenneville, J., Taylor, R.S., van Duin, A.C.T., 2010. Reactive molecular dynamics studies of DMMP adsorption and reactivity on amorphous silica surfaces. J. Phys. Chem. C 114, 18894. https://doi.org/10.1021/jp104547u.

Rodríguez, D.F.M., Saul, L., Wurz, P., Fuselier, S.A., Funsten, H.O., McComas, D.J., Möbius, E., 2012. IBEX-Lo observations of energetic neutral hydrogen atoms originating from the lunar surface, Planet. Space Sci 60 (1), 297–303. https://doi.org/10.1016/j.pss.2011.09.009.

Saito, Y., Delcourt, D., Hirahara, M., et al., 2021. Pre-flight Calibration and Near-Earth Commissioning Results of the Mercury Plasma Particle Experiment (MPPE) Onboard MMO (Mio). Space Sci. Rev 217, 70. https://doi.org/10.1007/s11214-021-00839-2.

Saito, Y., Yokota, S., Tanaka, T., Asamura, K., Nishino, M.N., Fujimoto, M., Tsunakawa, H., Shibuya, H., Matsushima, M., Shimizu, H., Takahashi, F., Mukai, T., Terasawa, T., 2008. Solar wind proton reflection at the lunar surface : low energy ion measurement by MAP-PACE onboard SELENE (KAGUYA). Geophys. Res. Lett. 35 (24). https://doi.org/10.1029/2008gl036077.

Sarantos, M., Tsavachidis, S., 2021. Lags in desorption of lunar volatiles. Astrophys. J. Lett. 919 (2), L14. https://doi.org/10.3847/2041-8213/ac205b.

Saul, L., Wurz, P., Vorburger, A., Rodríguez, M.D.F., Fuselier, S.A., McComas, D.J., Möbius, E., Barabash, S., Funsten, H.O., Janzen, P., 2013. Solar wind reflection from the lunar surface: the view from far and near. Planet. Space Sci. 84, 1–4. https://doi.org/10.1016/j.pss.2013.02.004, 2013.

Schaible, M.J., Dukes, C.A., Hutcherson, A.C., Lee, P., Collier, M.R., Johnson, R.E., 2017. Solar wind sputtering rates of small bodies and ion mass spectrometry detection of secondary ions. J. Geophys. Res.: Planets 122, 1968–1983. https://doi.org/10.1002/2017JE005359.

Smith, R., Jolley, K., et al., 2017. A ReaXFF carbon potential for radiation damage studies. Nucl. Instrum. Methods Phys. Res. B 393, 49. https://doi.org/10.1016/j.nimb.2016.11.007.

Stern, S.A., 1999. The lunar atmosphere: history, status, current problems and context. Rev. Geophys. 37 (4), 453–491.

Szabo, P., et al., 2022a. Graphical user interface for SDTrimSP to simulate sputtering, ion implantation and the dynamic effects of ion irradiation. NIMB 522, 47–53. https://doi.org/10.1016/j.nimb.2022.04.008.

Szabo, P., et al., 2022b. (a) deducing lunar regolith porosity from energetic neutral atom emission. Geophys. Res. Lett. 49. https://doi.org/10.1029/2022GL101232.

Thomas, E.W., Janev, R.K., Smith, J., 1992. Scaling of particle reflection coefficients. Nucl. Instrum. Methods Phys. Res. Sect. B Beam Interact. Mater. Atoms 69 (4), 427–436. https://doi.org/10.1016/0168-583x(92)95298-6.

Thompson, A.P., M Aktulga, H., et al., 2022. LAMMPS - a flexible simulation tool for particle-based materials modeling at the atomic, meso, and continuum scales. Comput. Phys. Commun. 271, 108171. https://doi.org/10.1016/j.cpc.2021.108171.

Vorburger, A., Wurz, P., Barabash, S., Wieser, M., Futaana, Y., Holmstr€om, M., Bhardwaj, A., Asamura, K., 2014. First direct observation of sputtered lunar oxygen. J. Geophys. Res. 119 (2), 709–722. https://doi.org/10.1002/2013JA019207.

Weissmann, R., Sigmund, P., 1973. Sputtering and backscattering of keV light ions bombarding random targets. Radiat. Eff. 19, 7. https://doi.org/10.1080/00337577308232208.

Wieser, M., Barabash, S., Futaana, Y., Holmström, M., Bhardwaj, A., Sridharan, R., Dhanya, M.B., Wurz, P., Schaufelberger, A., Asamura, K., 2009. Extremely high reflection of solar wind protons as neutral hydrogen atoms from regolith in space. Planet. Space Sci. 57 (14–15), 2132–2134. https://doi.org/10.1016/j.pss.2009.09.012.

Wieser, M., Barabash, S., Futaana, Y., Holmström, M., Bhardwaj, A., Sridharan, R., Dhanya, M.B., Wurz, P., Schaufelberger, A., Asamura, K., 2011. Erratum to "Extremely high reflection of solar wind protons as neutral hydrogen atoms from regolith in space [Planet. Space Sci. 57 (2009) 2132–2134] Planet. Space Sci. 59, 798–799. https://doi.org/10.1016/j.pss.2011.01.016, 2011.

Yu, Y., Wang, B., et al., 2016. Revisiting silica with ReaxFF: towards improved predictions of glass structure and properties via reactive molecular dynamics. J Non Cryst. Sol. 443, 148. https://doi.org/10.1016/j.jnoncrysol.2016.03.026.

Zhang, A., Wieser, M., Wang, C., Barabash, S., Wang, W., Wang, X., et al., 2020. Emission of energetic neutral atoms measured on the lunar surface by Chang'E-4. Planet. Space Sci. 189 (15). https://doi.org/10.1016/j.pss.2020.104970.

Ziegler, J.F., 2004. SRIM-2003. Nucl. Instrum. Methods B 219–220, 1027. https://doi.org/10.1016/j.nimb.2004.01.208.